isvr Institute of Sound and Vibration Research

A Comparison of a Theoretical Model for Quasi-statically and Dynamically Induced Environmental Vibration from Trains with Measurements

X. Sheng, C.J.C. Jones and D.J. Thompson

ISVR Technical Memorandum No 865

August 2001

University of Southampton

SCIENTIFIC PUBLICATIONS BY THE ISVR

Technical Reports are published to promote timely dissemination of research results by ISVR personnel. This medium permits more detailed presentation than is usually acceptable for scientific journals. Responsibility for both the content and any opinions expressed rests entirely with the author(s).

Technical Memoranda are produced to enable the early or preliminary release of information by ISVR personnel where such release is deemed to the appropriate. Information contained in these memoranda may be incomplete, or form part of a continuing programme; this should be borne in mind when using or quoting from these documents.

Contract Reports are produced to record the results of scientific work carried out for sponsors, under contract. The ISVR treats these reports as confidential to sponsors and does not make them available for general circulation. Individual sponsors may, however, authorize subsequent release of the material.

UNIVERSITY OF SOUTHAMPTON

INSTITUTE OF SOUND AND VIBRATION RESEARCH

DYNAMICS GROUP

A Comparison of a Theoretical Model for Quasi-statically and Dynamically Induced Environmental Vibration from Trains with Measurements

by

X. Sheng, C.J.C. Jones and D.J. Thompson

ISVR Technical Memorandum No: 865

August 2001

Authorized for issue by
Dr M.J. Brennan
Group Chairman

ABSTRACT

The subject of ground vibration generated by railways on the ground surface has received greatly increased attention in recent years. The new interest lies particularly in high-speed lines where train speeds may exceed the propagation velocities of Rayleigh wave modes in the soil. For environmental vibration, however, it is still the case that slow heavy-axle load traffic on conventional lines gives rise to the majority of complaints about vibration in line side buildings.

This paper considers vibration generation by a series of moving axle loads of the train and also by the dynamic forces generated by the irregular profile of the track. It presents a theoretical model for vibration generation and propagation that encompasses both these mechanisms of excitation. The vertical dynamics of a number of vehicles travelling at a constant speed on an infinite track are coupled to a semi-analytic model for a three-dimensional layered ground.

Using this model, ground vibration at three sites are predicted and compared with measured data. The comparisons show a reasonable correspondence although an analysis of the sensitivity of some of the parameters shows that, due to the inherent uncertainty in these parameters, the quality of such a comparison is bound to be limited.

This model also demonstrates the roles of the two components of vibration at different frequencies and for train speeds below and above the lowest ground wave speed. It is found that, in most practical cases, the dynamic component gives rise to higher levels of vibration.

CONTENTS

1. INTRODUCTION

The problem of ground vibrations generated by surface trains has received intense attention in the past few years. A seminar was held focussing on ground vibrations induced by high-speed trains in March 2000 at Gothenburg, Sweden [1]. At this seminar, about 50 researchers from different countries exchanged their experiences on the topic. At the workshop WAVE 2000 held in December 2000 at Bochum, Germany, a large proportion of the papers were devoted to ground vibration from railway trains [2]. A number of models have therefore been reported for predicting ground vibrations from trains [e.g., 3 to 6]. The new interest lies particularly in high-speed lines where train speeds may exceed the propagation velocities of Rayleigh wave modes in the soil. Thus, amongst the three mechanisms of generation of ground vibration [6], which are moving axle (quasi-static) loads, stationary dynamic forces and moving dynamic forces, most of the models only take into account the first one, i.e., the moving axle loads. For environmental vibration, however, it is still the case that slow heavy-axle load traffic on conventional lines gives rise to the majority of complaints about vibration in line side buildings. Ground vibration induced by moving axle loads is independent of the dynamics of vehicles and of track quality. However, it is known that, at least in some circumstances, these do have an effect on the level of vibration. In fact, reference [7] shows that the prediction using such models underestimates the actual response level, especially for higher excitation frequencies.

The dynamic excitations at wheel-rail contact points come from the irregular vertical profiles of the wheel and the rail running surfaces. Rail irregularities include joints, corrugations and the general undulations in the 'track top'. Wheel irregularities include wheel flats, surface irregularities and wheel eccentricity. The variations in the vertical profiles of either surface (wheel and rail) introduce a relative displacement input to the vehicle and track systems. The process is usually assumed to be linear, so that for a given wavelength, a displacement input is generated at the passing frequency. Hence a wavelength λ generates a frequency of excitation $f = c / \lambda$, where c denotes the train speed. For the frequency range of 5 Hz to 80 Hz, which is of interest for the perception of ground vibration, and a train speed range of 36 to 250 km/h (10 to 70 m/s), the important wavelengths lie within the range of 0.125 to 14 m (or wave number from 0.07 to 8 m^{-1}).

Comprehensive analysis requires realistic models of ground vibration generation and propagation. This model should be able to account for the interactions between vehicles, track and ground, and for the effect of train speeds.

This paper considers vibration generation by a series of moving axle loads of the train and also by the dynamic forces generated by the irregular profile of the track. It presents a theoretical model for vibration generation and propagation that encompasses both these mechanisms of excitation. The vertical dynamics of a number of vehicles travelling at a constant speed on an infinite track are coupled to a semi-analytic model for a three-dimensional layered ground. Using this model, ground vibration is predicted at three sites and compared with measured data. The model is also used to demonstrate the roles of the two components of vibration at different frequencies and for train speeds below and above the lowest ground wave speed.

In section 2, the modelling approach is outlined briefly. Sections 3 to 5 are devoted to the prediction and comparison for the three sites. Based on these predictions and comparisons, discussions are given in section 6.

2. OUTLINE OF THE MODEL

The model consists of three subsystems: vehicles, a track and a ground. A diagram of the subsystems is shown in figure 1.

Each vehicle is modelled as a multi-body system but only vertical dynamics is considered. As shown in figure 1, M_C and J_C denote the mass and the pitch inertia of the car body, and M_B and J_B denote those of each bogie. Boxes containing a cross represent the suspensions. The dynamic stiffness of the secondary suspension per bogie is denoted by k_2, while that of the primary suspension per axle is denoted by k_1. For each wheelset, M_W denotes its mass.

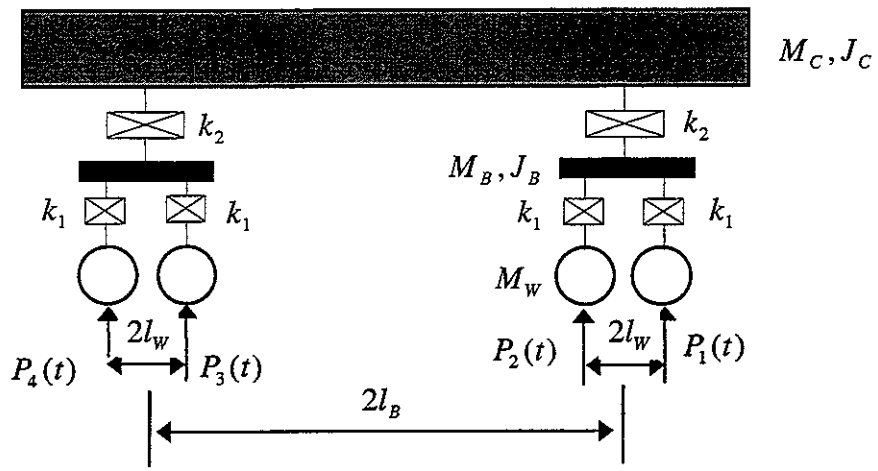

(a)

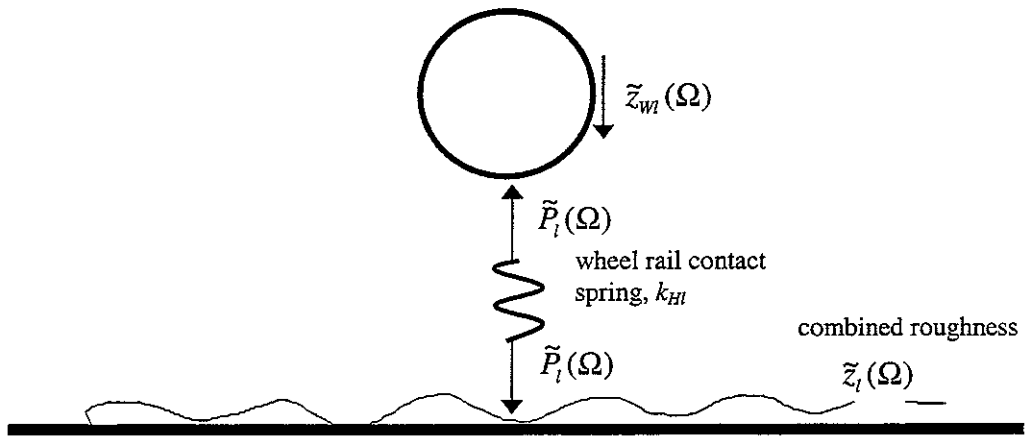

(b)

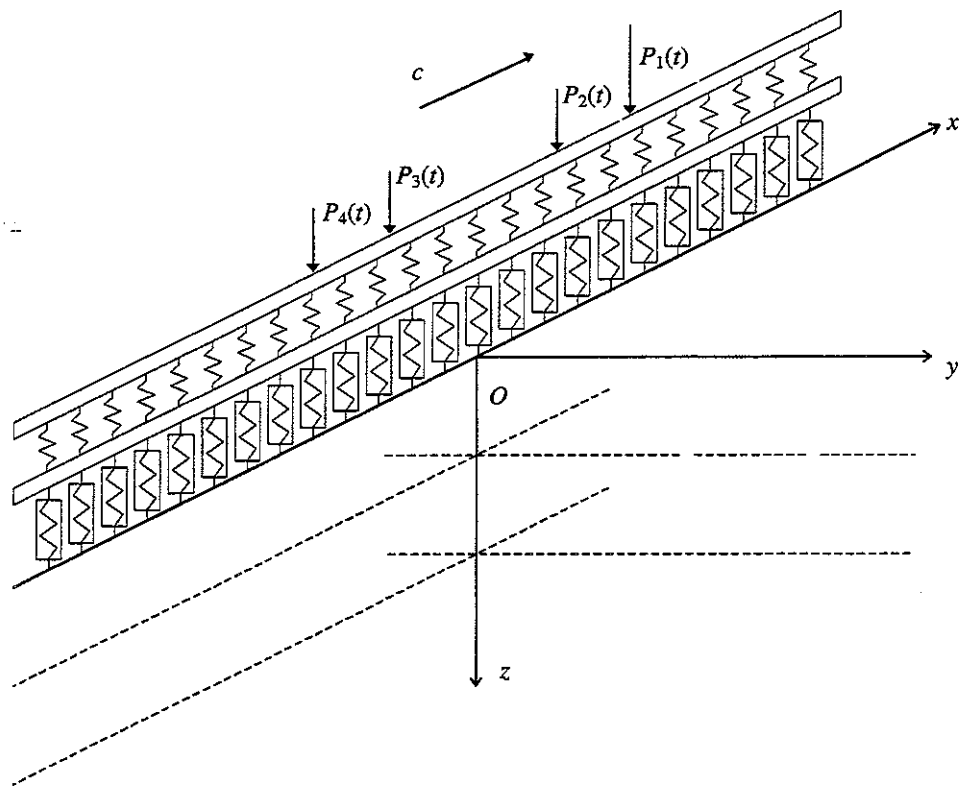

(c)

Figure 1. The vehicle-track-ground system. (a) a vehicle, (b) coupling of a wheelset with the rail, (c) the track-ground sub-system

The model for the railway track is the same as that used in reference [6]. The track is aligned in the x direction. From the first wheelset of the first vehicle to the last wheelset of the last vehicle, the vertical wheel-rail forces are denoted by $P_1(t), P_2(t), \cdots, P_M(t)$, where M is the number of these forces. At time $t = 0$, the longitudinal co-ordinates of these forces are denoted by $a_1, a_2, \cdots, a_M$. The forces move along the rails uniformly at the train speed c. For each wheel-rail force, there are two components: one is a moving static axle load (called the quasi-static load) and the other is a moving dynamic load excited by the combined wheel-rail irregularities. The responses to the quasi-static loads are independent of the dynamics of the vehicles. The vertical displacement of the rail is denoted by $w_R(x,t)$.

As in reference [6], the ground may consist of a number, n, of layers. Underneath the nth layer a homogeneous half-space or a rigid foundation may be present. For particles on the ground surface, the vertical (z-direction), lateral (y-direction) and longitudinal (x-direction) displacements are denoted by $u_{10}(x,y,t)$, $v_{10}(x,y,t)$ and $w_{10}(x,y,t)$, respectively.

When a unit vertical harmonic load of angular frequency Ω is applied at the rails and moves at speed c, (when $t = 0$, the x-coordinate of the load position is zero) the steady-state displacement of the rails and the ground surface may be expressed as

$$\left.\begin{aligned} w_R(x,t) &= w_R^{\Omega}(x-ct)e^{i\Omega t} \\ w_{10}(x,y,t) &= w_{10}^{\Omega}(x-ct,y)e^{i\Omega t} \end{aligned}\right\} \tag{1}$$

For a single wavelength of rail irregularity, λ, the vehicles vibrate harmonically at frequency $\Omega = 2\pi c/\lambda$, and the wheel-rail forces can be expressed as $P_l(t) = \tilde{P}_l(\Omega)e^{i\Omega t}$, where, $l = 1, 2, \cdots, M$. The responses of the rails and the ground surface due to this rail irregularity are given by summarizing those induced by each wheel-rail force, i.e.,

$$\left.\begin{aligned} w_R(x,t) &= \sum_{k=1}^{M} w_R^{\Omega}(x-a_k-ct)\tilde{P}_k(\Omega)e^{i\Omega t} \\ w_{10}(x,y,t) &= \sum_{k=1}^{M} w_{10}^{\Omega}(x-a_k-ct,y)\tilde{P}_k(\Omega)e^{i\Omega t} \end{aligned}\right\} \tag{2}$$

From equation (2), the amplitude of the displacement of the lth wheel/rail contact point on the rails, denoted by $\tilde{z}_{Rl}(\Omega)$, is given by letting $x = a_l + ct$ in equation (2):

$$\tilde{z}_{Rl}(\Omega) = \sum_{k=1}^{M} \sigma_{lk}^{R} \tilde{P}_k(\Omega) \tag{3}$$

where,

$$\sigma_{lk}^{R} = w_R^{\Omega}(a_l - a_k) \tag{4}$$

which is the transfer receptance between the lth and the kth wheel/rail contact point on the rails. It should be pointed out that, due to the motion of the loads, $\sigma_{lk}^{R} \neq \sigma_{kl}^{R}$.

Similarly, the displacement amplitude of the lth wheelset, denoted by $\tilde{z}_{Wl}(\Omega)$, can be expressed as

$$\tilde{z}_{Wl}(\Omega) = \sum_{k=1}^{M} \sigma_{lk}^{T} \tilde{P}_k(\Omega) \tag{5}$$

where, σ_{lk}^{T} is determined by the parameters of the vehicles and is the transfer receptance between the lth wheelset and the kth wheelset, and $\sigma_{lk}^{T} = \sigma_{kl}^{T}$.

It is assumed that each wheelset is always in contact with the rails. This requires that (see figure 1(b))

$$\sum_{k=1}^{M} (\sigma_{lk}^{T} + \sigma_{lk}^{R}) \tilde{P}_k(\Omega) + \frac{1}{k_{Hl}} \tilde{P}_l(\Omega) = -\tilde{z}_l(\Omega) \quad (l = 1,2,\cdots,M) \tag{6}$$

where, k_{Hl} denotes the stiffness of the Hertz contact spring between the lth wheelset and the rails, and $\tilde{z}_l(\Omega)$ denotes the amplitude of the rail irregularity of the wavelength considered. From equation (6), the wheel/rail forces can be calculated. Thus the displacements of the track and the ground surface are completely determined by substituting the wheel/rail forces into equation (2). It should be noted that for $\Omega = 0$, each wheel-rail force is equal to the relevant static axle load.

The displacement spectra of the rails and the ground surface are obtained by performing Fourier transformation on equation (2) with respect to time t. Denoting the vertical displacement spectrum of point (x, y) on the ground surface by $S_w(x, y, f)$, where f is the frequency at which the spectrum is evaluated, it can be shown that

$$S_w(x, y, f) = S_w^0(x, y, f; \Omega) S_P(f; \Omega) \tag{7}$$

where,

$$S_w^0(x,y,f;\Omega) = \int_{-\infty}^{\infty} w_{10}^{\Omega}(x-ct,y)e^{i\Omega t}e^{-i2\pi ft}\,dt \tag{8}$$

which is the vertical displacement spectrum of the ground surface due to a unit harmonic load of frequency Ω moving at speed c along the rails.

$$S_P(f;\Omega) = \sum_{l=1}^{M} \tilde{P}_l(\Omega)e^{-ia_l(\Omega-2\pi f)/c} \tag{9}$$

is a 'load spectrum' describing the frequency content of the excitation associated with the moving multiple loads.

The vertical irregular profile of the rails is normally described by its power spectral density, $P_z(\beta)$, where, β denotes the wave number in radians. For each wave number (or each wavelength) of a discrete spectrum of the rail irregularity, the displacement spectrum of the ground can be evaluated using equation (7). The total displacement spectrum of the ground is equal to the sum of those for each wavelength of the rail irregularity. In equation (6), let $\tilde{z}_l(\Omega) = 1$. Then it can be shown that, the total vertical displacement power spectrum on the ground surface, denoted by $P_w(x,y,f)$, is given by

$$\begin{aligned} P_w(x,y,f) = & |S_w^0(x,y,f;0)|^2 |S_P(f;0)|^2 \\ & + \frac{1}{2\pi}\sum_{k=1}^{\infty}\{|S_w^0(x,y,f;\Omega_k)|^2 |S_P(f;\Omega_k)|^2 + \\ & + |S_w^0(x,y,f;-\Omega_k)|^2 |S_P(f;-\Omega_k)|^2\}P_z(\beta_k)\Delta\beta \end{aligned} \tag{10}$$

where, $\beta_k = k\Delta\beta$, $\Omega_k = \beta_k c$. In equation (10), the first part corresponds to the power spectrum generated by the quasi-static loads while the second part is due to track irregularities. When divided by a chosen period of time, which normally is the time needed for the whole train to pass a fixed point, equation (10) gives an estimation of the vertical displacement power spectral density (PSD) of the ground surface.

3. SIMULATIONS AND COMPARISON FOR SITE I

First the model is applied to predict the train-induced vibration for the X2000 high-speed train. The Swedish National Rail Administration (BANVERKET) encountered very large vibrations when its X2000 high-speed trains (figure 2) were operated at 200 km/h at a site called Ledsgård. This site is located on the West Coast line south of Gothenburg. BANVERKET carried out an extensive program of measurements with a test train in order to investigate the causes of the high level of vibrations. It was observed that when the train speed approached the 'Rayleigh wave' velocity of the ground, an extraordinarily strong response occurs [1]. The soil properties of the site are listed in table 1, the track parameters are in table 2 and the axle loads of the test train and their locations are in table 3. The values of parameters in these three tables have all been taken to be those identified by BANVERKET in its measurement programme [8]. As indicated in table 1, the ground at this site is modelled as two layers on a homogeneous half-space, and the second layer, consisting of organic clay, is very soft.

TABLE 1
The ground parameters for the Ledsgård site [8]

Layer	Depth (m)	Young's modulus (10^6 Nm^{-2})	Poisson's ratio	Density (kg/m^3)	Loss factor	P-wave speed (m/s)	S-wave speed (m/s)
1	1.6	19.0	0.491	1500	0.15	500	65
2	3.0	3.84	0.498	1250	0.15	500	32
Half-space		31.82	0.498	1470	0.15	1500	85

TABLE 2
The parameters for a ballasted railway track [8]

Mass of rail beam per unit length of track	120 kg/m
Bending stiffness of rail beam	1.26×10^7 N-m^2
Loss factor of the rail	0.01
Rail pad stiffness per unit length of track	3.5×10^8 N/m^2
Rail pad loss factor	0.15
Mass of sleepers per unit length of track	490 kg/m
Mass of ballast per unit length of track	1200 kg/m
Ballast stiffness per unit length of track	3.15×10^8 N/m^2
Loss factor of ballast	0.2
Density of the embankment	1800 kg/m^3
Young's Modulus of the embankment	2.95×10^8 N/m^2
Loss factor of the embankment	0.3
Top width of the embankment	2.7 m
Height of the embankment	0.9 m
Contact width of railway and ground	3 m

TABLE 3
Axle locations and axle loads [8]

No.	1	2	3	4	5	6	7	8	9	10
a_j (m)	50.00	47.10	35.50	32.60	28.25	25.35	10.60	7.65	3.30	0.40
P_j (KN)	167.50	119.00	143.25	143.25	122.00	122.00	122.00	122.00	125.50	125.50
No.	11	12	13	14	15	16	17	18	19	20
a_j (m)	-14.40	-17.30	-21.65	-24.54	-39.35	-42.25	-46.60	-49.50	-56.10	-59.00
P_j (KN)	125.50	125.50	122.00	122.00	122.00	122.00	185.75	185.75	183.00	188.50

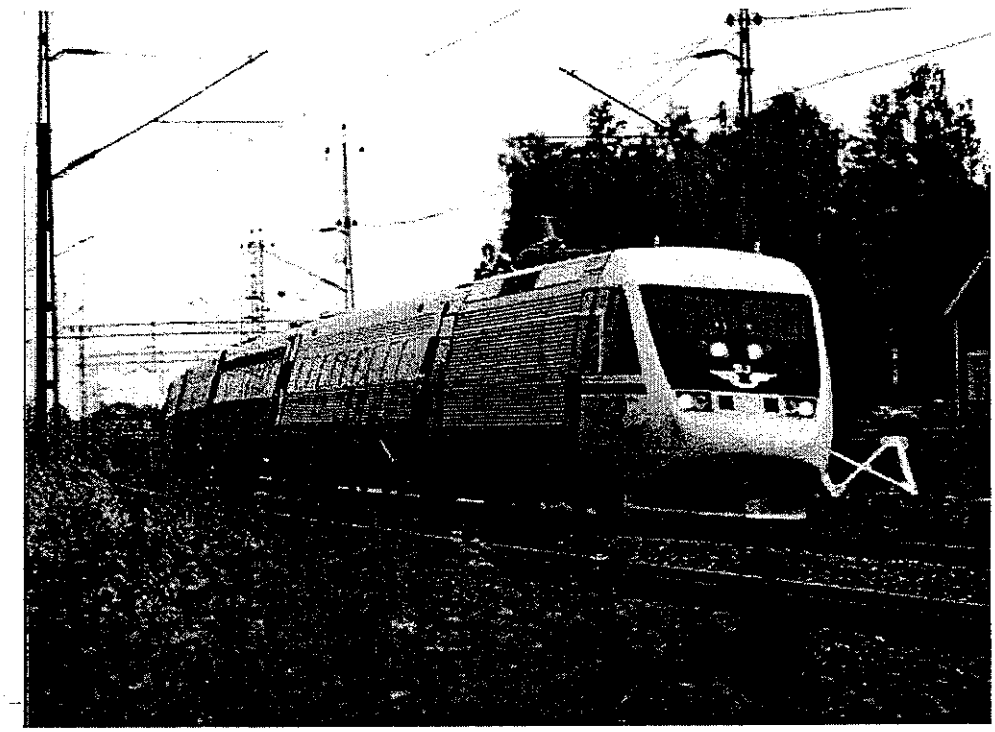

Figure 2. The X2000 high-speed train

In sub-section 3.1 below, the dispersion curves of the ground are calculated. Mode shapes are plotted in sub-section 3.2 for propagating wave modes of the ground at several frequencies. In sub-section 3.3, the displacements of the embankment under the action of the test train at two speeds, 70 km/h and 200 km/h, are predicted and compared with measured data. Predicted and measured velocity spectra of the ground surface are compared in sub-section 3.4.

3.1 DISPERSION CURVES OF THE GROUND

Figure 3 shows the P-SV dispersion curves of the ground at Ledsgård for a frequency range of 0 to 50 Hz. Here only the real wavenumbers of the first five modes are plotted from an undamped eigenvalue analysis of the system at each frequency. The curves therefore indicate the presence of propagating waves and near-field waves are not

shown. It can be seen that: (1) the cut-on points are always on the shear wave line of the underlying half-space; (2) for higher frequencies, the wave of the first mode (i.e. the mode with the highest wave number at a given frequency) approaches the shear wave of the second layer; (3) The shear wave line of the first layer intersects the dispersion curves at their inflection points.

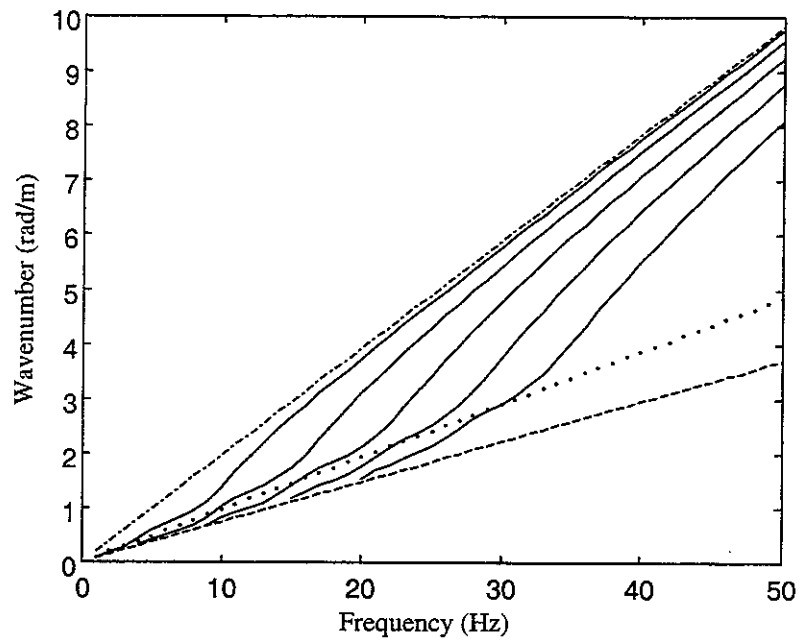

Figure 3. Dispersion curves for the ground at Ledsgård site. ——, P-SV modes; – – –, shear wave of the underlying half-space; · · · · · ·, shear wave of the upper layer; – · – · –, shear wave of the second layer.

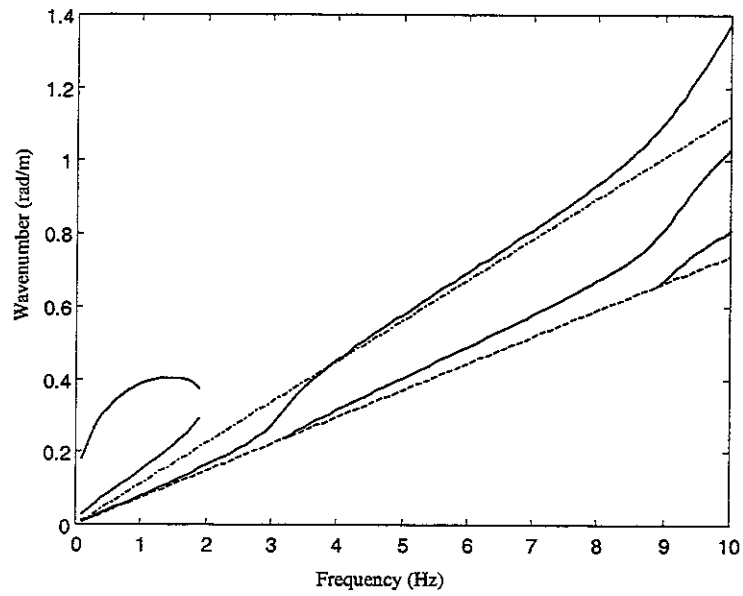

Figure 4. P-SV dispersion curves of the ground at Ledsgård site. ——, P-SV modes; – – –, shear wave of the half-space; – · – · –, the load speed line for a speed of 55.6 m/s.

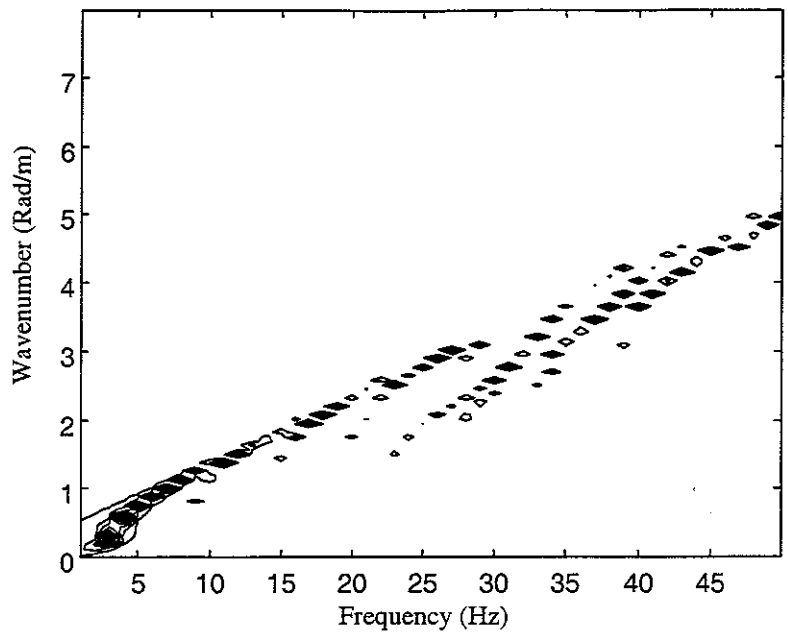

Figure 5. Contour plot of the Fourier transformed vertical displacement on the ground surface.

An enlarged dispersion curve diagram for a small range of frequency of 0 Hz to 10 Hz is shown in figure 4. A complex characteristic of the ground is revealed by this figure. Below 2 Hz, three wave modes are available while between 2 and 3.3 Hz, only one wave mode is present. Also shown in this figure is a 'load speed line' indicating the excitation of modes by a moving constant load (see [6] and [9]).

The dispersion curves may be produced by the Fourier transformed displacements on the ground surface due to a surface harmonic load of different frequencies. Figure 5 shows the contour plot of the transformed vertical displacements on the ground surface due to a vertical surface point load of different frequencies. This plot has a speckled appearance because of the discrete frequencies of excitation applied in the calculation. Compared with figure 3, this figure shows that waves are only excited which have speeds greater than the Rayleigh wave speed in the first layer but less than the shear wave speed in the underlying half-space. Other waves propagate along the interface of the second layer and the half-space and decay so rapidly away from the interface (see below) that they do not contributes significantly to the forced surface response.

3.2 MODE SHAPES OF THE GROUND

The P-SV mode shapes are calculated and shown in figure 6 to figure 9 for the first mode at frequencies 1.4 Hz, 1.9 Hz, 3 Hz and 20 Hz. The layer interfaces are also indicated using horizontal lines. As shown in figures 6 and 7, the mode shapes in the underlying half-space resemble the mode shape of the Rayleigh wave in the same half-

space, and the ground surface has minimum displacement. In figure 9, the first mode at 20 Hz, only propagates near the interface of the second layer and the half-space. However, figure 8 shows that at 3 Hz, the ground has maximum displacement at its surface. Thus, when a load speed is just over the shear wave speed of the second layer, the load speed line would intersects the dispersion curve of the first mode at high frequency (see figure 3). Because of the mode shape at high frequency (figure 9), the ground surface response induced by this moving load is not expected to be very large. On the other hand, when the load speed is close to the shear wave speed of the first layer, the load speed line intersects, or is very close to, the dispersion curve of the first mode at about 3 to 8 Hz (figure 4). In this case, the ground surface response is expected to be very strong. Both measurement and simulation show this, as presented in the following subsections.

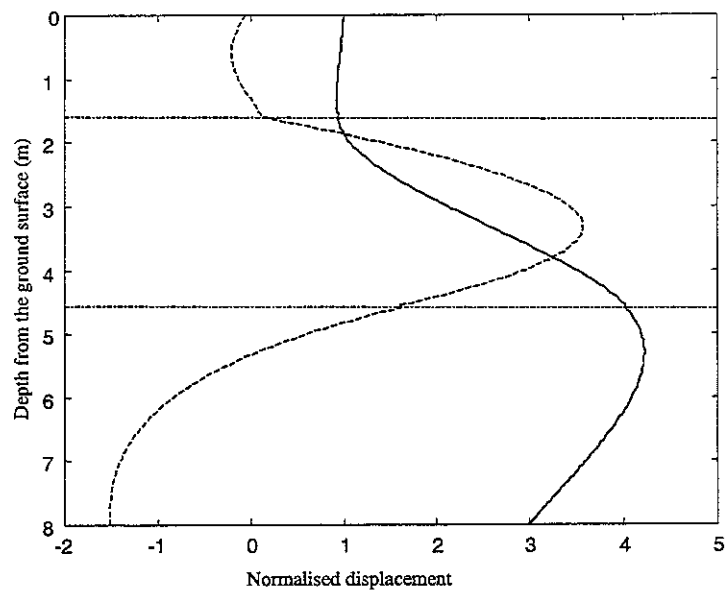

Figure 6. The first P-SV mode shape (frequency = 1.4 Hz, wavenumber = 0.4 rad/m) for the ground at Ledsgård site. ——, vertical component; – – –, horizontal component.

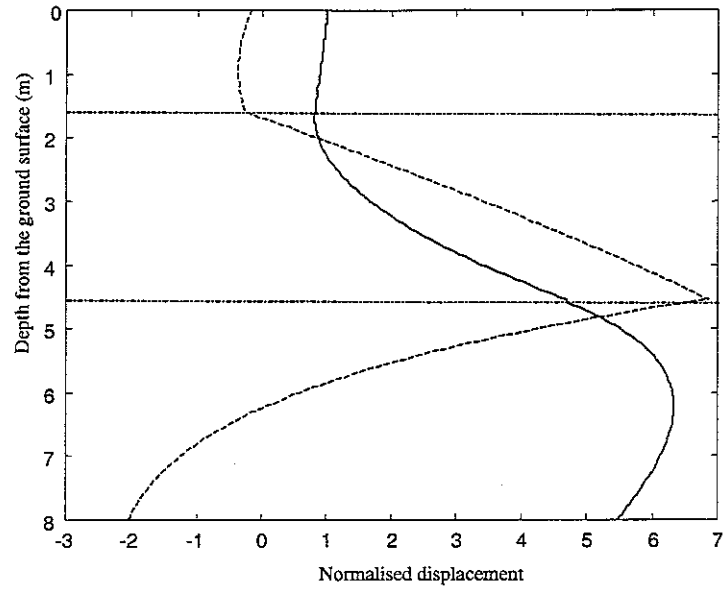

Figure 7. The P-SV mode shape (frequency = 1.9 Hz, wavenumber = 0.375 rad/m) for the ground at Ledsgård site. ——, vertical component; – – –, horizontal component.

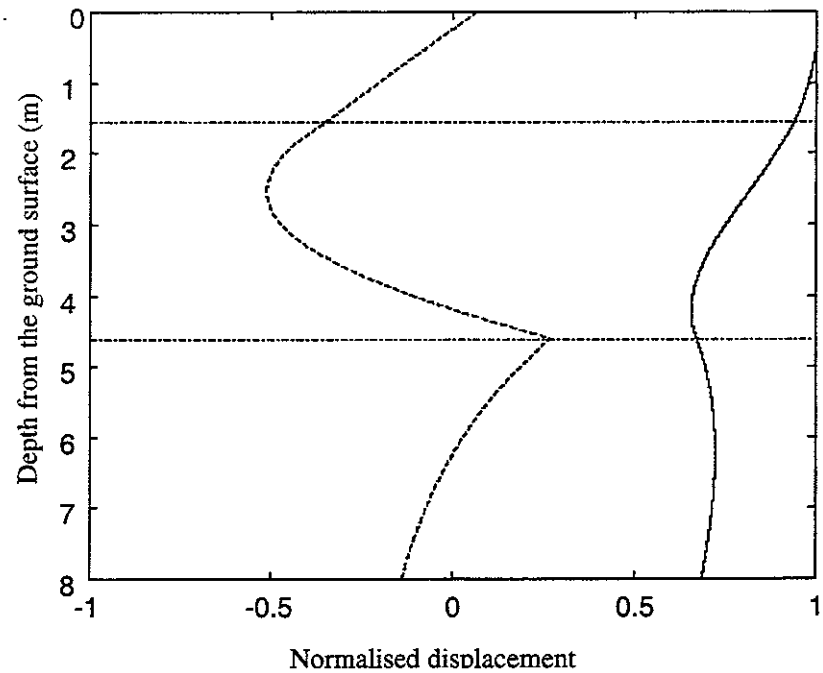

Figure 8. The P-SV mode shape (frequency = 3 Hz, wavenumber = 0.272 rad/m) for the ground at Ledsgård site. ——, vertical component; – – –, horizontal component.

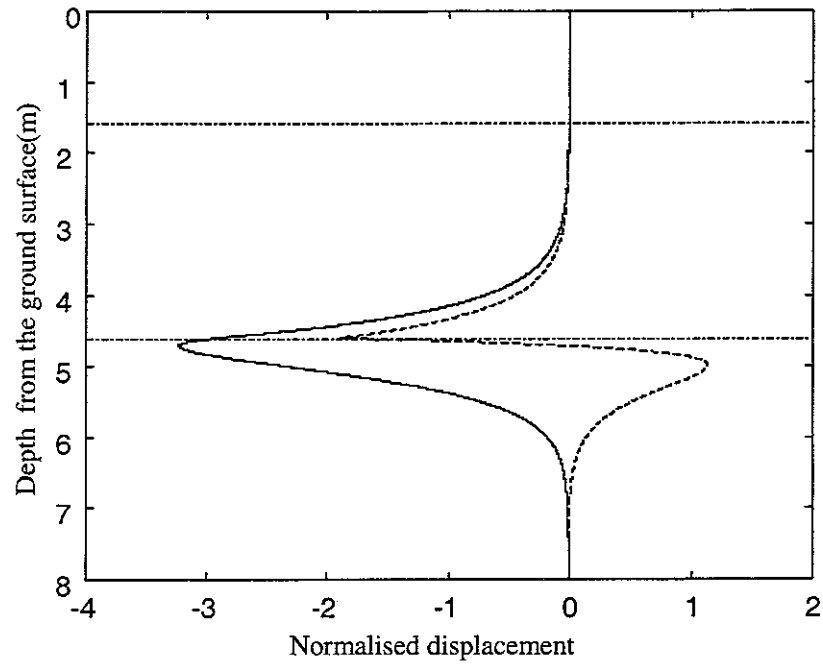

Figure 9. The P-SV mode shape of the first mode (frequency = 20 Hz, wavenumber = 3.74 rad/m) for the ground at Ledsgård site. ——, vertical component; – – –, horizontal component.

3.3 DISPLACEMENTS OF THE TRACK GENERATED BY THE QUASI-STATIC LOADS

Simulations are performed for the displacements generated by the X2000 test train. Two train speeds, 70 km/h (19.4 m/s) and 200 km/h (55.6 m/s), are considered. In these predictions, only the quasi-static loads are taken into account. The magnitudes and locations of the axle loads are listed in table 3. Figure 10 shows the instantaneous displacements of the embankment at 70 km/h and figure 11, at 200 km/h. At the track the response to the dynamic wheel-rail forces is expected to be small compared to the moving axle loads. The success of the prediction indicates the accuracy of the ground and track parameters derived by BANVERKET [8]. For the low speed case shown in figure 10, a quasi-static loading state is clearly indicated. However, in the high-speed case, a propagating wave mode is excited and a large oscillating response appears because of the excitation of this propagating wave mode. As shown in figure 4, the load speed line for a load speed equal to 200 km/h (55.6 m/s) has an intersection with the dispersion curve of the first mode at a wave number of 0.4 rad/m. The presence of the mass of the track (including an embankment) will decrease this wavenumber to some extent. As a result, a propagating wave of more than 16 m wavelength is excited in the track and propagates away from each load in the reverse direction of the train motion

(compare results shown in reference [6]). Behind the last axle load, a wave 'tail' of this wavelength is clearly visible in figure 11.

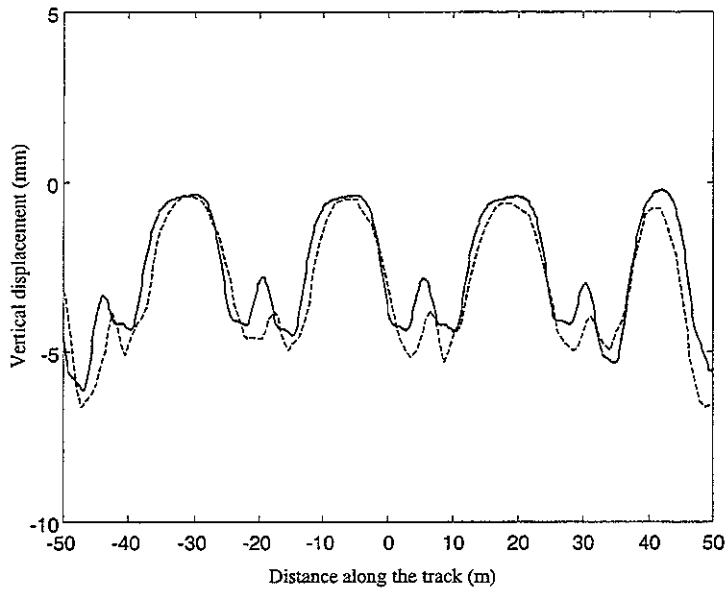

Figure 10. Predicted (——) and measured (– – –) vertical displacement of the embankment for train speed equal to 70 km/h (19.4 m/s)

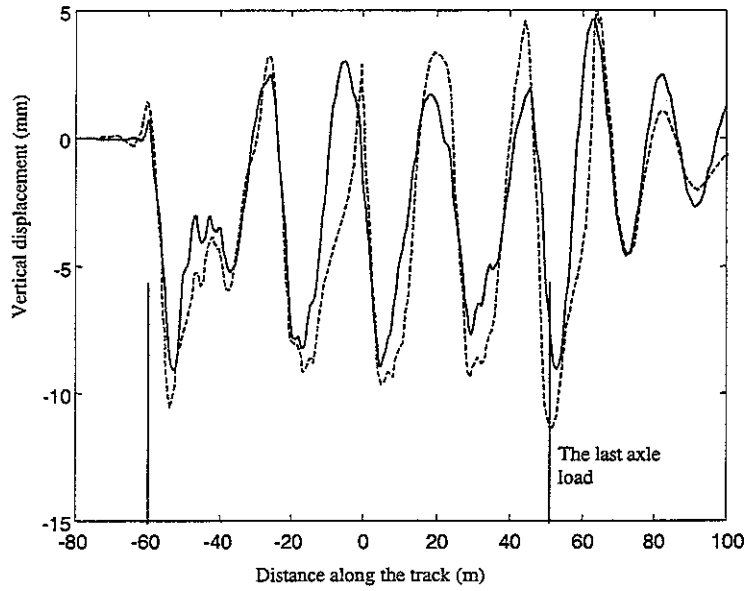

Figure 11. Predicted (——) and measured (– – –) vertical displacement of the embankment at 200 km/h (55.6 m/s).

3.4 VELOCITY SPECTRA OF THE GROUND SURFACE GENERATED BY THE QUASI-STATIC LOADS

3.4.1 *FOR TRAIN SPEED* 70 km/h

The predicted load spectrum, given by equation (9), for the X2000 test train moving at 70 km/h is shown in figure 12. Predicted and measured velocity spectra of vibration on the track are compared in figure 13. Figures 14 and 15 show the results for locations on the ground surface 7.5 m and 15 m away from the track centre line. The measurements were carried out using seismometers with a natural frequency of 2 Hz. It can be seen from figure 13 that on the embankment, for frequencies higher than 5 Hz and lower than 22 Hz, the prediction reproduces the measurement quite well. It indicates that for the response of the track, the quasi-static loads are the dominating sources over the dynamic loads. However, as shown in figures 13 and 14, away from the track on the ground surface, the predicted response is much lower than the measured one.

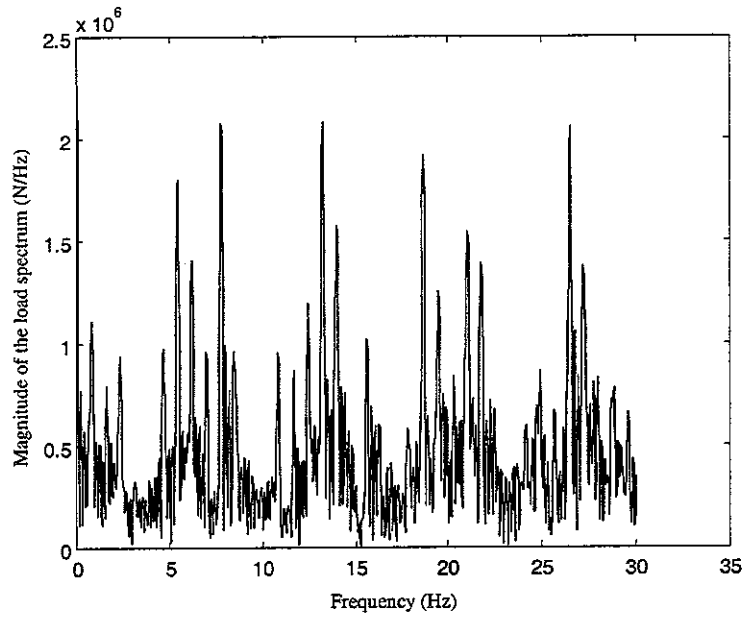

Figure 12. Load spectrum of the multiple quasi-static loads for train speed 70 km/h (19.4 m/ s) calculated from equation (9) with $\Omega = 0$.

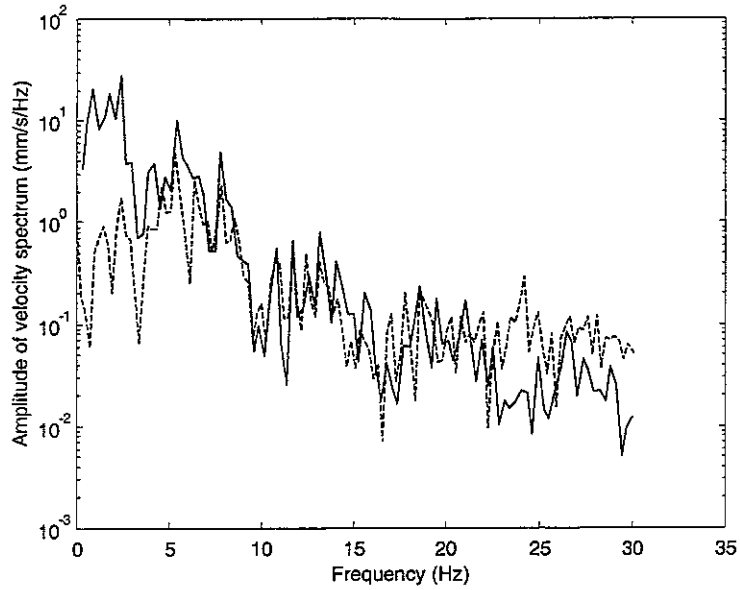

Figure 13. Vertical velocity spectrum of the embankment. ——, predicted; – – –, measured. Train speed: 70 km/h (19.4 m/s).

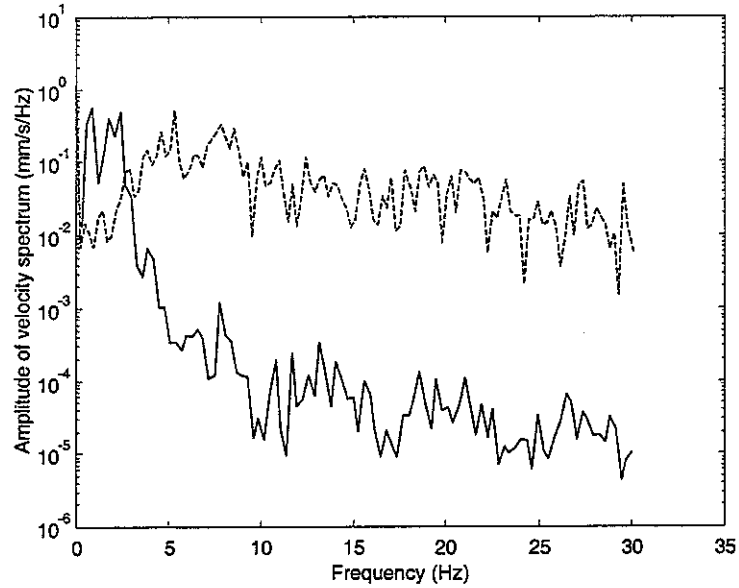

Figure 14. Vertical velocity spectrum for a point 7.5 m away from the track centre line on the ground surface. ——, predicted; – – –, measured. Train speed: 70 km/h (19.4 m/s).

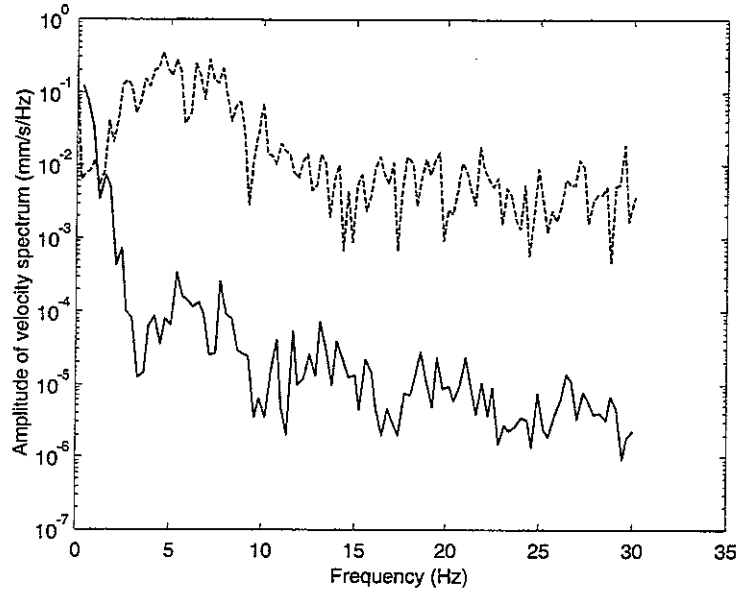

Figure 15. Vertical velocity spectrum for a point 15 m away from the track centre line on the ground surface. ——, predicted; – – –, measured. Train speed: 70 km/h (19.4 m/s).

3.4.2 *FOR TRAIN SPEED* 200 km/h

Figures 16 to 19 show the predicted and measured vertical velocity spectra of different points on the ground surface for the test train running at 200 km/h. It can be seen that at low frequencies and for points near the track, for example the point 7.5 m away from the track, the predicted responses are quite close to the measured ones. This is quite different from the low speed case shown in figure 14. However, at higher frequencies, especially at further distances from the track, the simulations underestimate the response. At frequencies around 3 to 8 Hz, even for points far from the track, the predicted responses are close to those measured. The harmonic components of such frequencies are due to the first propagating wave mode excited by the moving quasi-static loads and correspond to the range of frequency at which the load speed line for 200 km/h (55.6 m/s) intersects, or is very close to, the dispersion curve of the first mode (figure 4).

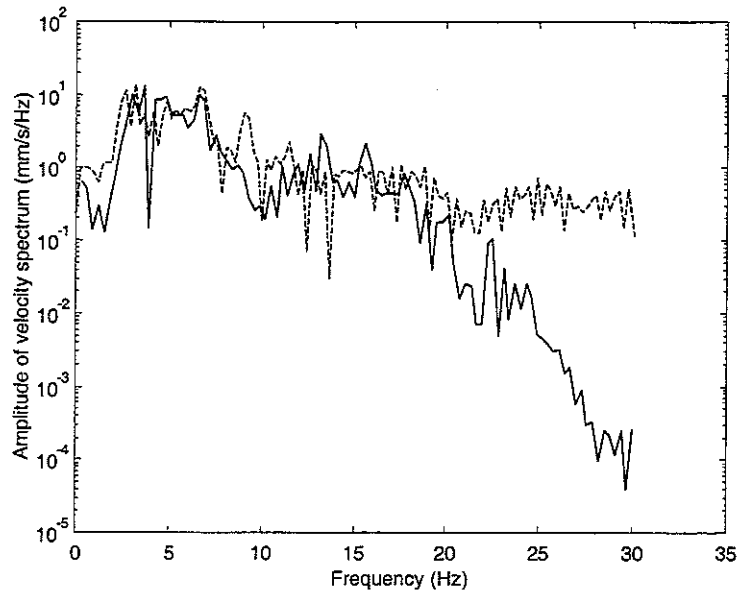

Figure 16. Vertical velocity spectrum for a point 7.5 m away from the track on the ground surface. ——, predicted; – – –, measured. Train speed: 200 km/h (55.6 m/s).

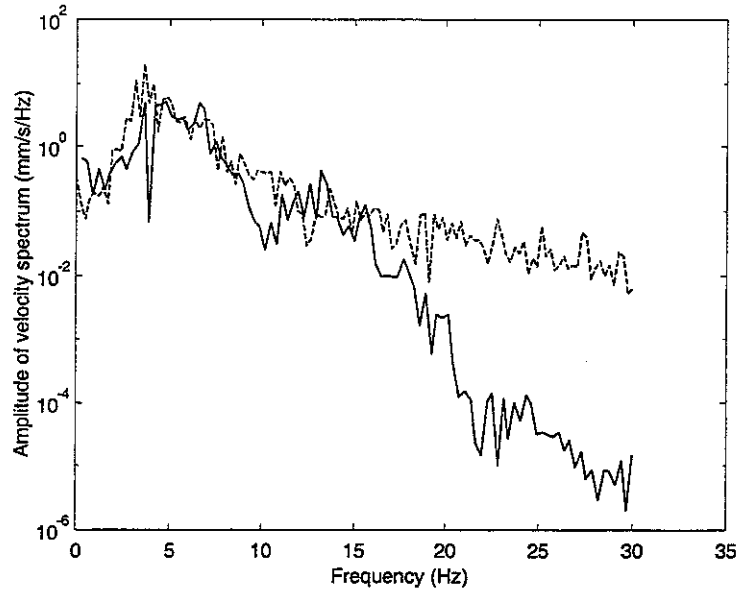

Figure 17. Vertical velocity spectrum for a point 15 m away from the track on the ground surface. ——, predicted; – – –, measured. Train speed: 200 km/h (55.6 m/s).

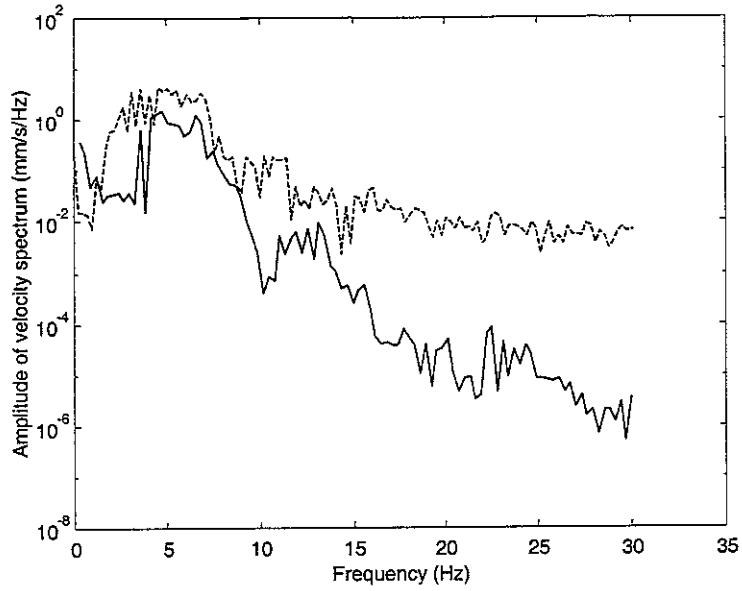

Figure 18. Vertical velocity spectrum for a point 30 m away from the track on the ground surface. ——, predicted; – – –, measured. Train speed: 200 km/h (55.6m/s).

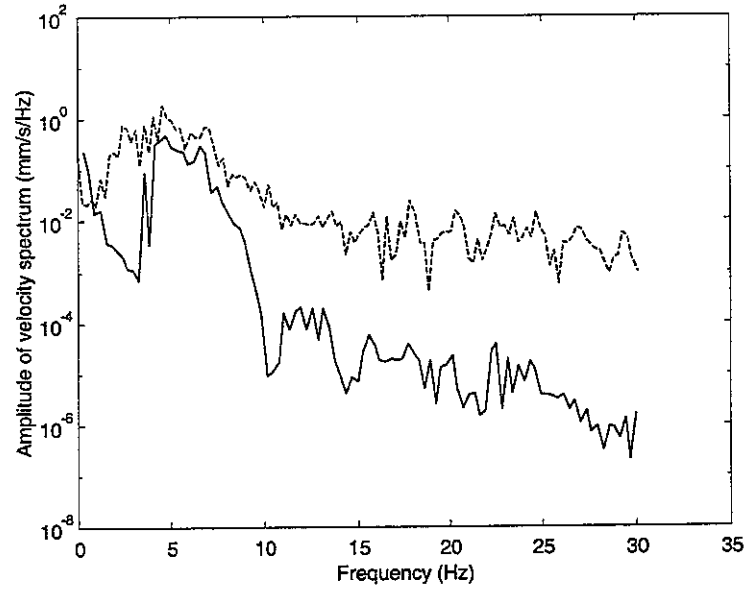

Figure 19. Vertical velocity spectrum for a point 45 m away from the track on the ground surface. ——, predicted; – – –, measured. Train speed: 200 km/h (55.6 m/s).

3.5 TOTAL VELOCITY SPECTRA GENERATED BY THE QUASI-STATIC AND DYNAMIC LOADS

As shown in section 3.4, the dynamic wheel-rail forces contribute a large proportion to the ground response. To predict the total response generated by the test train, the vehicle suspension parameters for the X2000 train have been provided by

BANVERKET (in confidence). In the absence of data specific to the site, the vertical rail-head profile for a nominally 'good' track measured on a 200 km/h mixed traffic main line in England has been used. The spectral density of this is shown in figure 20. The vertical irregularities of the wheels also, to some extent, contribute to the ground vibration. Most conventional wheels used in main line vehicles have rolling radii varying from 0.4 to 0.5 m. For operational train speeds varying from 10 m/s to 70 m/s, wheel out-of-round produces an excitation with a fundamental frequency ($f = c / (2\pi R)$) ranging from 4 to 22 Hz, i.e., within the frequency range of interest. However, since wheel out-of-round data are not available, this has not been included in the irregularity data used in any of the predictions in this paper.

The vertical velocity levels of two points on the ground surface for two train speeds are shown in figures 21 to 24. Though without specific irregularity data, the prediction does not reproduce the measurement very well, it can clearly be concluded that for train speeds lower than the wave speeds in the ground at this site, the dynamic components of the wheel-rail forces are dominant over the quasi-static loads even for very low frequencies. However, for train speeds exceeding the wave speeds in the ground, the quasi-static loads are dominating for frequencies up to more than 10 Hz.

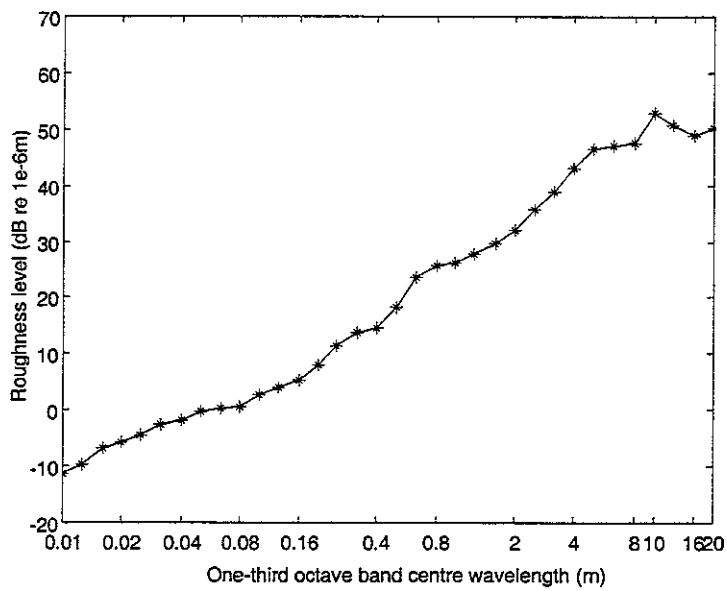

Figure 20. Rail roughness level used in the prediction.

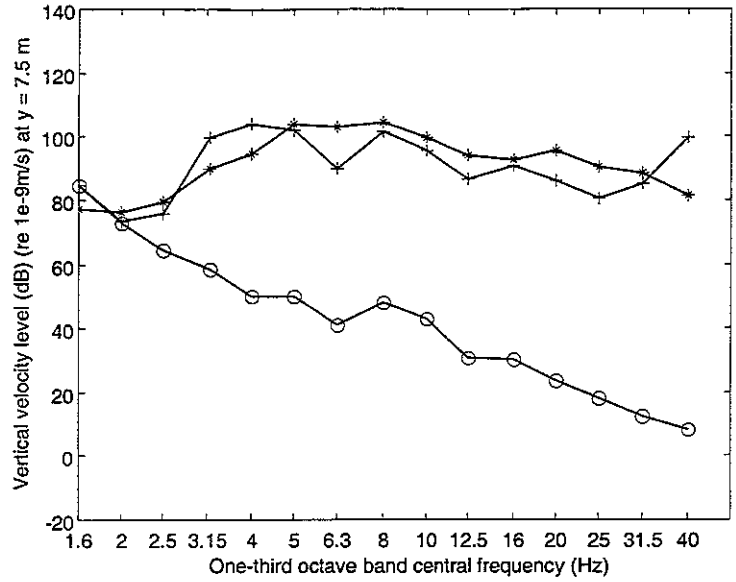

Figure 21. Vertical velocity level for a point 7.5 m from the track on the ground surface. o: predicted level due to quasi-static loads; +: predicted total level; *: measured level. Train speed: 70 km/h (19.4 m/s).

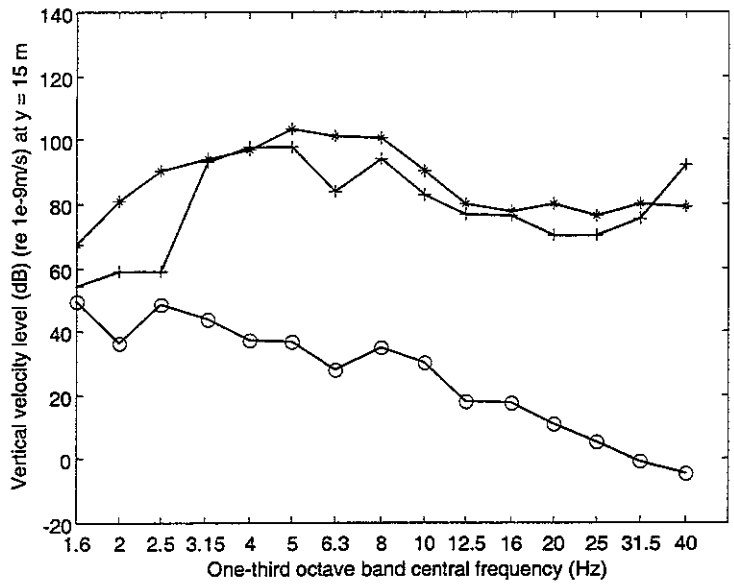

Figure 22. Vertical velocity level for a point 15 m from the track on the ground surface. o: predicted level due to quasi-static loads; +: predicted total level; *: measured level. Train speed: 70 km/h (19.4 m/s).

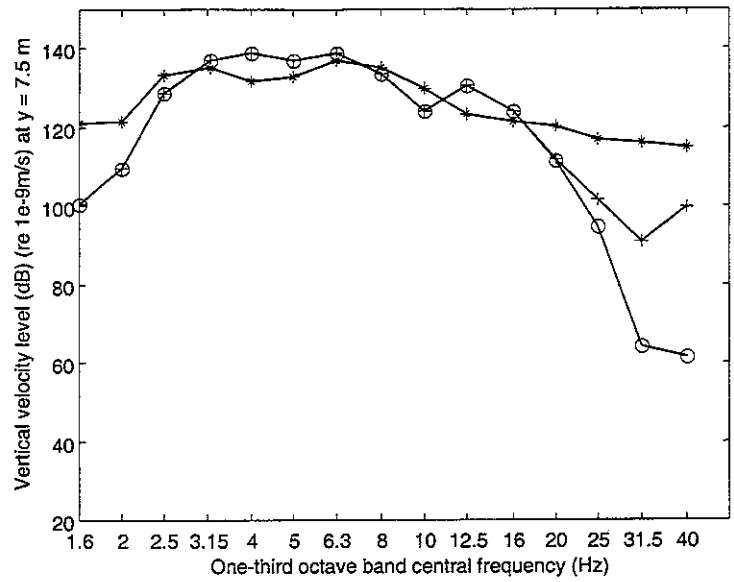

Figure 23. Vertical velocity level for a point 7.5 m from the track on the ground surface. o: predicted level due to quasi-static loads; +: predicted total level; *: measured level. Train speed: 200 km/h (55.6 m/s).

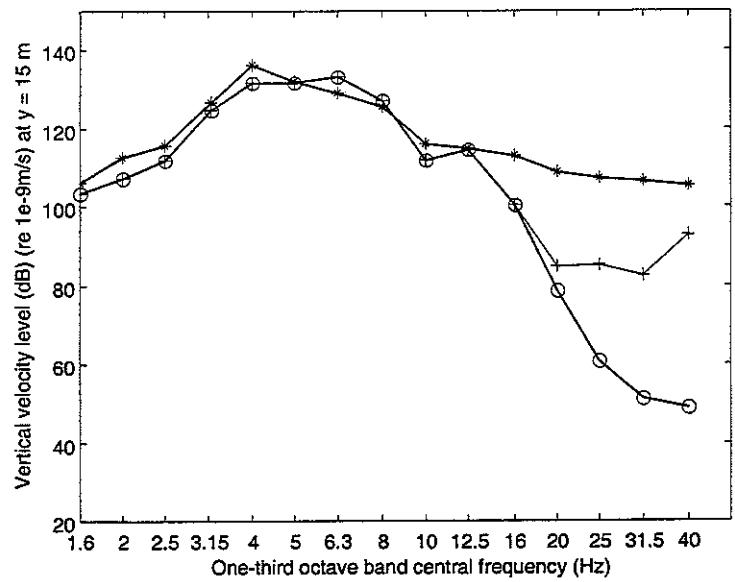

Figure 24. Vertical velocity level for a point 15 m from the track on the ground surface. o: predicted level due to quasi-static loads; +: predicted total level; *: measured level. Train speed: 200 km/h (55.6 m/s).

4. SIMULATIONS AND COMPARISON FOR SITE II

In this section, the model is applied to ground vibrations induced by the ETR500 high-speed train. A picture of the ETR500 train is shown in figure 25. Predicted vibration spectra are compared with vibration measurements carried out by Lai et al in November 1999, in Florence, Italy [7]. The transducers used in the measurements are geophones with a natural frequency of 2 Hz. A correction to the amplitudes around and below this frequency was applied in the original measurements. The average speed of the train passages during the measurement is about 70 to 80 km/h. The data measured at a site called Via Tedalda are used here for comparison. The parameters used for the vehicles, soil and track are listed in tables 4 to 6. According to figure 5 in reference [7], the ground is modelled as one layer of 10 m depth which overlies a homogenous half-space. The shear wave speeds in the layer and in the half-space are 300 m/s and 600 m/s, respectively. In the absence of specific parameters, the track structure, other than the embankment, has been assigned parameters typical of a monobloc sleeper, ballasted track. As advised by the authors of reference [7], the embankment is 1.5 m high, and its density has been estimated as 1800 kg/m^3. Since the Young's modulus of the embankment is uncertain, several values have been tested. It was found that the value (2.0×10^7 N/m^2) giving the closest correspondence with the measurement is that derived from the total vertical stiffness of the track, 50500 kN/m^2, suggested in reference [7]. In the simulations, five ETR500 passenger cars running at 25 m/s are coupled with the track-ground system and, again in the absence of specific data, the rail roughness data shown in figure 20 is used.

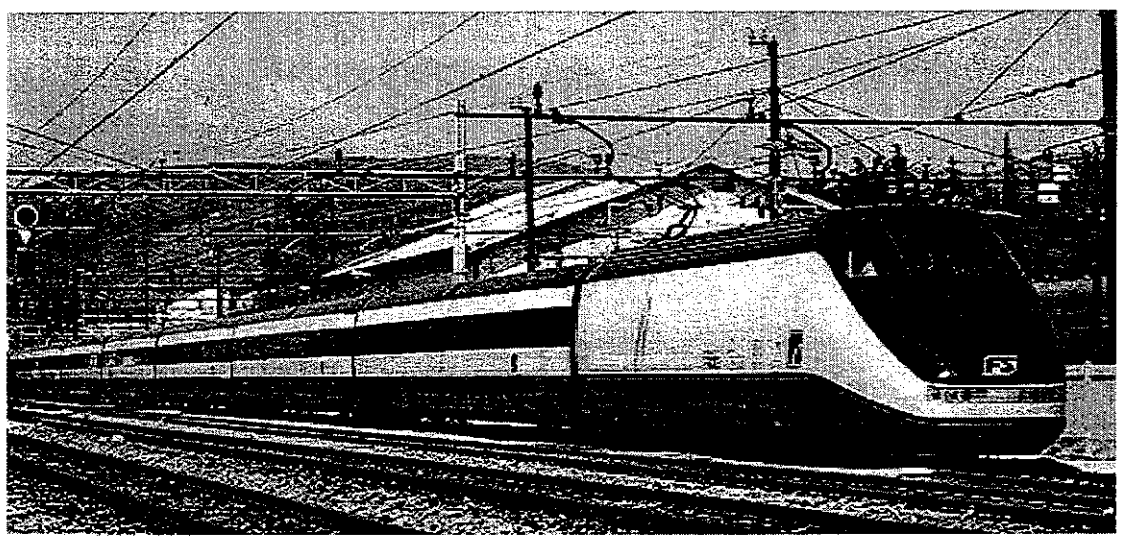

Figure 25. The ETR500 high-speed train.

The dispersion curves of the ground are shown in figure 26. As indicated in this figure, the cut-on frequency of the first propagating wave in the layer is 11.2 Hz.

Figures 27 and 28 show the amplitude spectra of the vertical component of the acceleration at distances of 13.0 m and 26.2 m from the track. The measured data are available as one-third octave spectra. The comparative predictions have therefore been band-averaged and are presented in the same way.

TABLE 4

The parameters of the vehicle (passenger coach)

Body mass (empty), (kg)	28440
Body pitch inertia (kg-m^2)	1.52×10^6
Bogie sprung mass (kg)	2820
Bogie pitch inertia (kg-m^2)	2843
Secondary vertical stiffness per bogie (N/m)	0.725×10^6
Secondary vertical damping per bogie (Ns/m)	6.37×10^4
Primary vertical stiffness per axle (N/m)	1.6×10^6
Primary vertical damping per axle (Ns/m)	2.2×10^4
Primary damper stiffness per axle (N/m)	14×10^6
Bogie centres (m)	2×9.5
Bogie wheelbase (m)	2×1.5
Wheelset mass (kg)	1420
Bogie centre (adjacent cars) (m)	7.1

TABLE 5

The ground parameters for Via Tedalda (in Italy) [7]

Layer	Depth (m)	Young's modulus (10^6 Nm^{-2})	Poisson's ratio	Density (kg/m^3)	Loss factor	P-wave speed (m/s)	S-wave speed (m/s)	Rayleigh wave speed (m/s)
1	10	469.8	0.45	1800	0.1	995	300	284
Half-space		1879.2	0.45	1800	0.1	1989.97	600	568.55

TABLE 6

The track parameters

Mass of rail beam per unit length of track	120 kg/m
Bending stiffness of rail beam	1.26×10^{7} N-m^2
Loss factor of the rail	0.01
Rail pad stiffness per unit length of track	3.5×10^{8} N/m^2
Rail pad loss factor	0.15
Mass of sleepers per unit length of track	490 kg/m
Mass of ballast per unit length of track	1200 kg/m
Ballast stiffness per unit length of track	3.15×10^{8} N/m^2
Loss factor of ballast	0.2
Density of the embankment	1800 kg/m^3
Young's Modulus of the embankment	2.0×10^{7} N/m^2
Loss factor of the embankment	0.05
Top width of the embankment	2.7m
Height of the embankment	1.5m
Contact width of railway and ground	4m

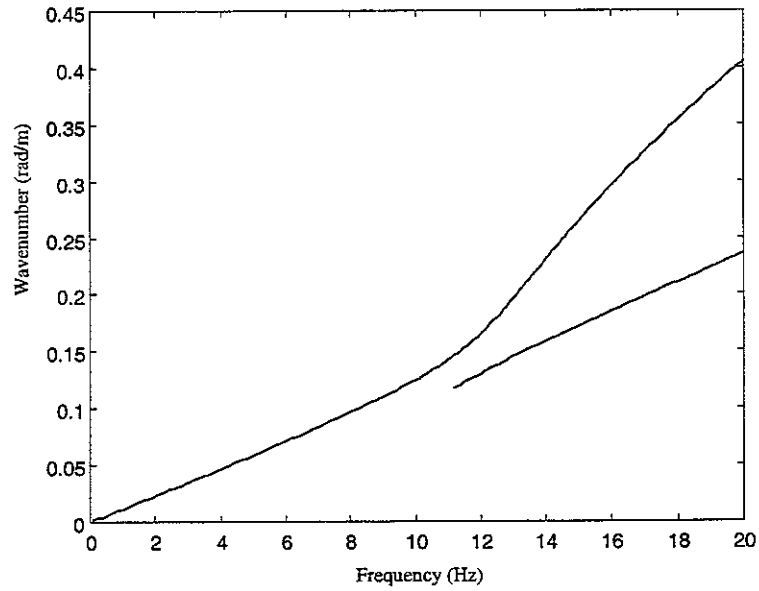

Figure 26. Dispersion curves of P-SV waves in the ground. Cut-on frequency is 11.2 Hz.

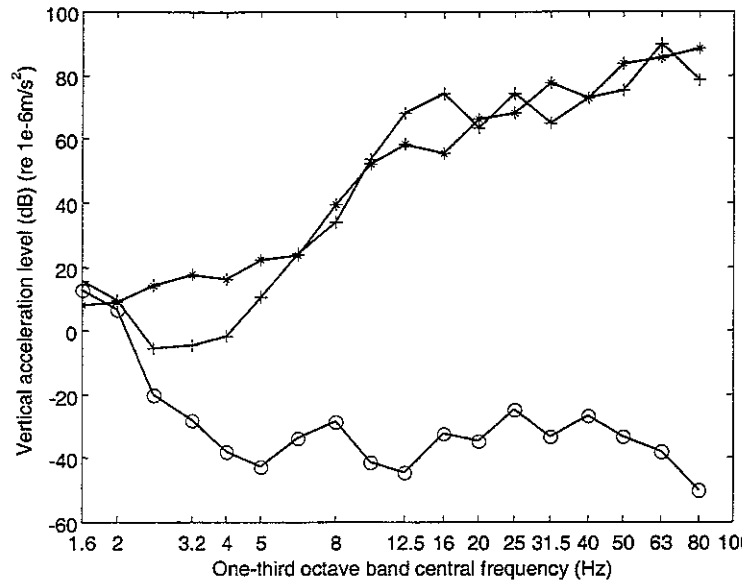

Figure 27. Vertical acceleration levels for a point 13 m from the track at Via Tedalda when five ETR 500 passenger cars pass at 25 m/s. o: predicted level due to quasi-static loads; +: predicted total level; *: measured level [7].

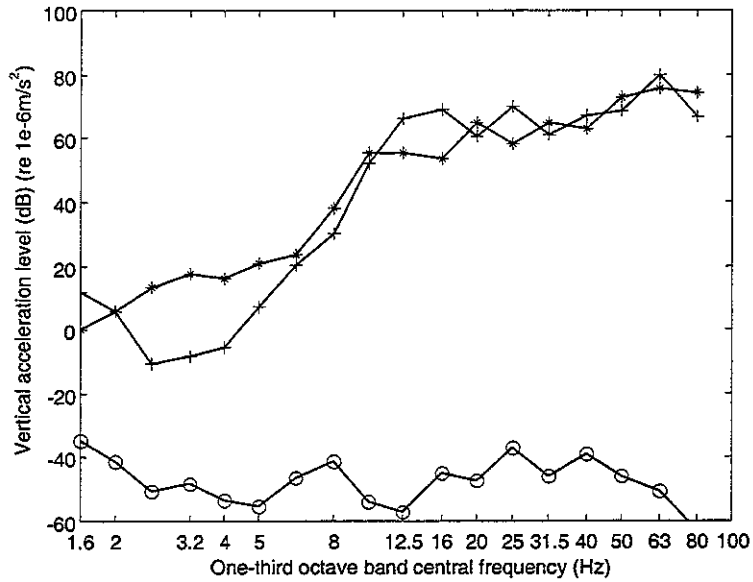

Figure 28. Vertical acceleration levels for a point 26.2 m from the track at Via Tedalda when five ETR 500 passenger cars pass at speed $c = 25$ m/s. o: predicted level due to quasi-static loads; +: predicted total level; *: measured level [7].

As seen in figures 27 and 28, both the prediction and the measurement show a strong rise in vibration level corresponding to the cut-on at about 12 Hz. This cut-on is due to the layered structure of the ground, as indicated by the dispersion diagram of the ground in figure 26. It is also shown that good correspondence is achieved between the

predicted response levels and the measured levels for frequencies higher than 5 Hz. However for frequencies of 2 to 5 Hz, the predicted levels are much lower than the measured ones. It is possible that this is due, in part, to a building near the track (figure 4 in reference [7]). Since the point 26.2 m away from the track is nearer the building, its effect may be stronger as shown in figure 28.

In the 12.5 and 16 Hz bands, the prediction is greater than the measurement in figures 27 and 28. This has been identified as due to the mathematical description of the ground as having a sudden change in stiffness at the layer-half-space interface. This is unrealistic for ground properties.

The effects of the variation in the Young's modulus of the embankment are shown in figure 29 and 30. Three values, 2×10^7 N/m^2, 5×10^7 N/m^2 and 10×10^7 N/m^2, are tested. Three frequency ranges are identified in figures 29 and 30: 1.6 to 5 Hz, 5 to 16 Hz, 16 to 80 Hz. It can be seen that increasing the Young's modulus of the embankment, the change in the response levels in the first frequency range are negligible, however, in the second frequency range, the response levels decrease with increasing stiffness of the embankment while in the third frequency range, they increase. It can be seen that the range of predictions encompassed by the uncertainty in the embankment stiffness alone covers the difference between the measurement and any individual prediction for frequencies above the cut-on frequency of the ground.

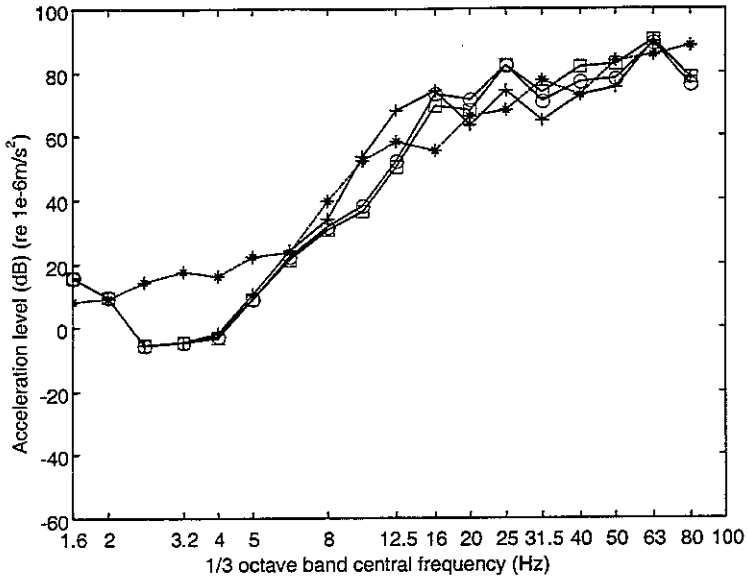

Figure 29. Effect of embankment Young's modulus on vertical acceleration levels at 13 m from the track at Via Tedalda when five ETR 500 cars run at 25 m/s. +: 2.0×10^7 N/m^2; o: 5.0×10^7 N/m^2; : 10.0×10^7 N/m^2; *: measured [7]

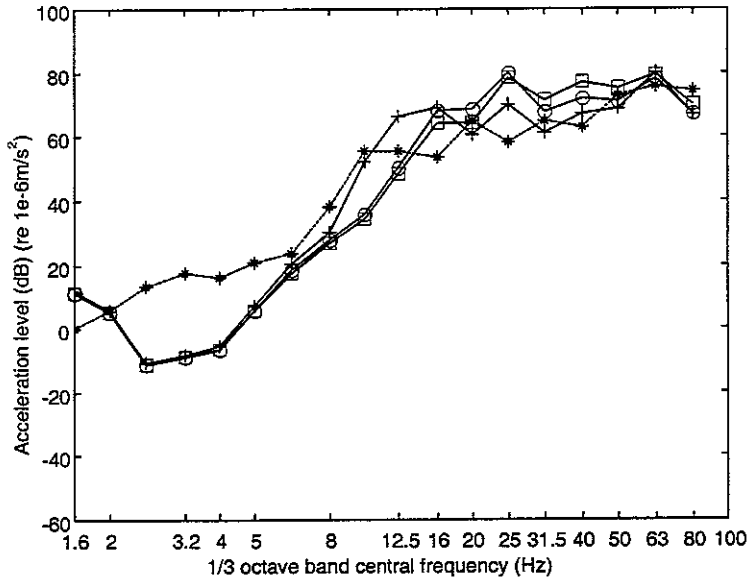

Figure 30. Effect of embankment Young's modulus on vertical acceleration levels at 26.2 m from the track at Via Tedalda when five ETR 500 cars run at 25 m/s. +: 2.0×10^7 N/m^2; o: 5.0×10^7 N/m^2; : 10.0×10^7 N/m^2; *: measured [7].

5. SIMULATIONS AND COMPARISON FOR SITE III

In this section, the model is applied to predict the vibrational spectra induced by a train of two-axle freight wagons (type HAA, figure 31). Again the prediction is compared with measured data. Information on the measurement at Burton Joyce in Nottinghamshire, England, is reported in reference [10]. The average speed of the train during the measurement is about 14 m/s. The parameters of vehicle, soil and track are listed in tables 7 to 9. According reference [10], the ground is modelled as a single layer of 1.8 m depth, which overlies a homogenous half-space. The shear wave speeds in the layer and in the half-space are 81 m/s and 216 m/s, respectively. The track is ballasted with an embankment of 1.3 m height. In this case, the rail roughness data specific to the site close to the time of the vibration measurement are available and shown in figures 32 and 33. It may be expected that for freight vehicles, wheel irregularity data may be more significant than for passenger stock. However, no data concerning the wheels is available.

TABLE 7

The parameters of the vehicle (HAA freight wagon)

Body mass (loaded), (kg)	42330
Body pitch inertia (kg-m^2)	1.7×10^5
Primary vertical stiffness per axle (N/m)	3.3×10^6
Primary vertical damping per axle (Ns/m)	2.0×10^5
Primary damper stiffness per axle (N/m)	100×10^6
Axle distance in a wagon (m)	2×2.781
Wheelset mass (kg)	1925
Wheel diameter (m)	0.92
Axle distance (adjacent wagons) (m)	3.08

TABLE 8

The ground parameters at Burton Joyce (in England) [10]

Layer	Depth (m)	Young's modulus (10^6 Nm^{-2})	Poisson's ratio	Density (kg/m^3)	Loss factor	P-wave speed (m/s)	S-wave speed (m/s)	Rayleigh wave speed (m/s)
1	1.8	29.3	0.47	1520	0.1	341	81	77
Half-space		286	0.49	2060	0.1	1700	216	206

TABLE 9

The parameters for a ballasted railway track in England (Burton Joyce) [10]

Mass of rail beam per unit length of track (BS 113A rail)	112 kg/m
Bending stiffness of rail beam	9.68×10^{6} N-m^2
Loss factor of the rail	0.01
Rail pad stiffness per unit length of track	3.5×10^{8} N/m^2
Rail pad loss factor	0.15
Mass of sleepers per unit length of track	396 kg/m
Mass of ballast per unit length of track	760 kg/m
Ballast stiffness per unit length of track	3.0×10^{8} N/m^2
Loss factor of ballast	0.2
Density of the embankment	1800 kg/m^3
Young's Modulus of the embankment	1.5×10^{7} N/m^2
Loss factor of the embankment	0.1
Top width of the embankment	2.7 m
Height of the embankment	1.3 m
Contact width of railway and ground	4 m

The P-SV mode dispersion diagram of the ground is calculated and shown in figure 34. As indicated, the first cut-on frequency is 15 Hz. The transfer mobilities (vertical responses due to vertical load) from ground to ground and from track to ground were measured by British Rail Research (now AEAT Rail) and are shown in figures 35 and 36. The measured responses in figure 35 show the variation in moving the loading point and the measurement point within a small area. Using the parameters in tables 7 to 8, the transfer mobility is predicted and the results are also shown in these two figures. Both the prediction and measurement show a strong rise at a frequency of about 15 Hz. A similar discrepancy is also observed at around 20 Hz between the model and the measurements to that observed at the Via Tedalda site because of the unrealistic sudden change in ground properties at the layer interface.

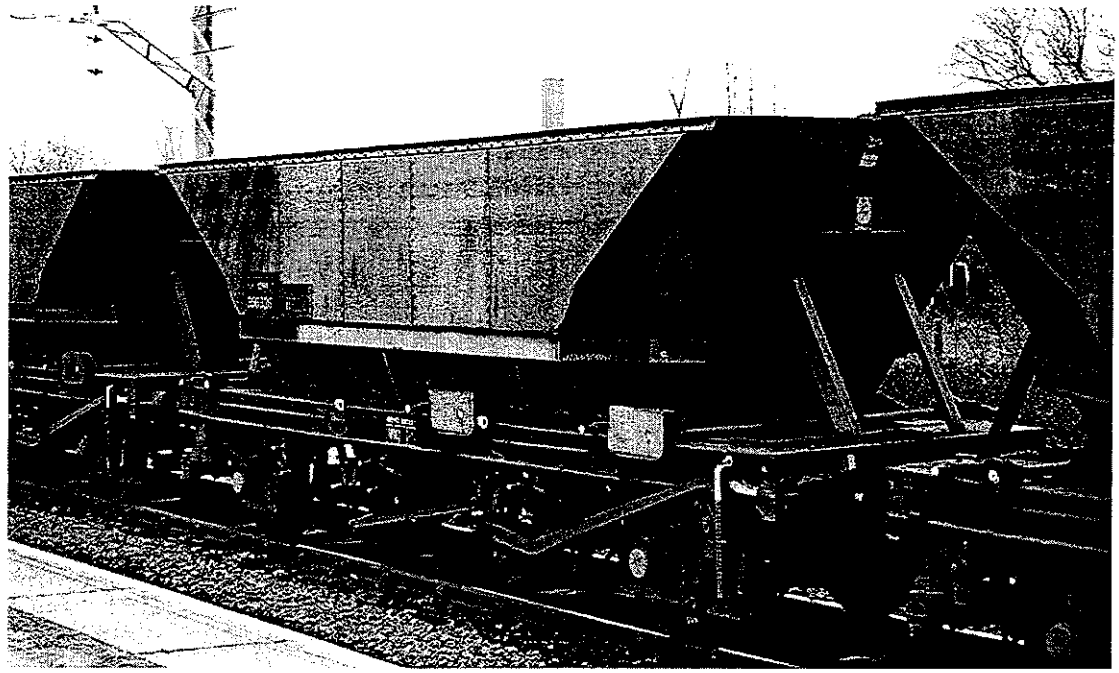

Figure 31. The HAA coal freight wagons

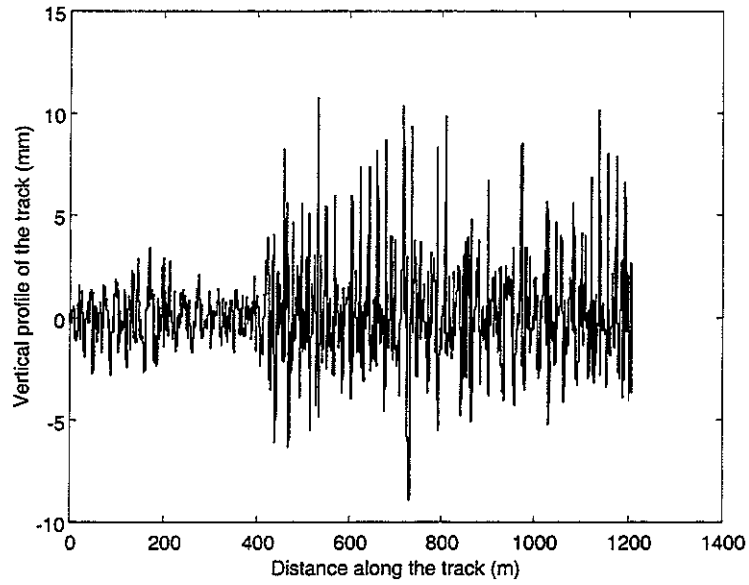

Figure 32. Vertical profile of the rail at Burton Joyce site.

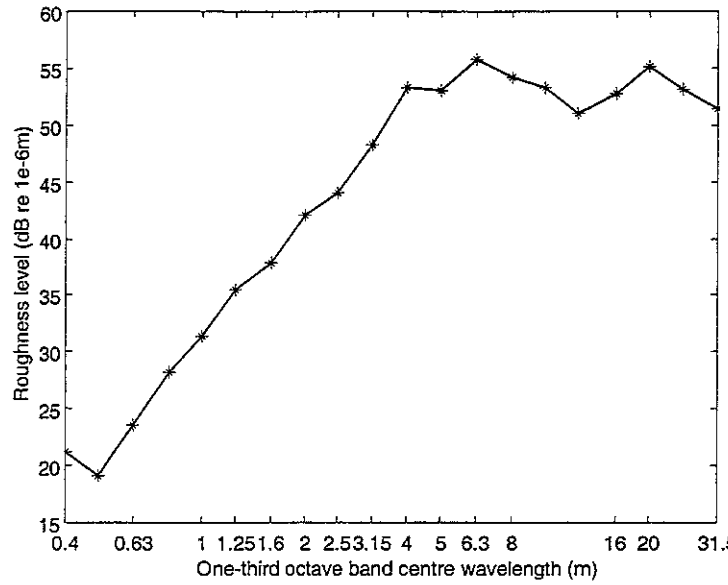

Figure 33. Spectrum of roughness of the rails at Burton Joyce site.

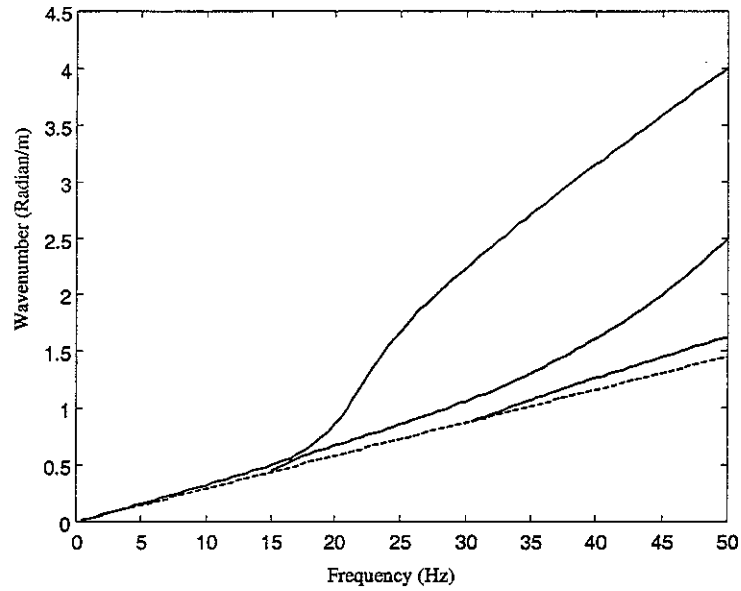

Figure 34. Dispersion curves of P-SV (——) waves in the ground. Cut-on frequencies are 15 Hz and 30 Hz. Also shown is the shear wave of the underlying half-space (– – –).

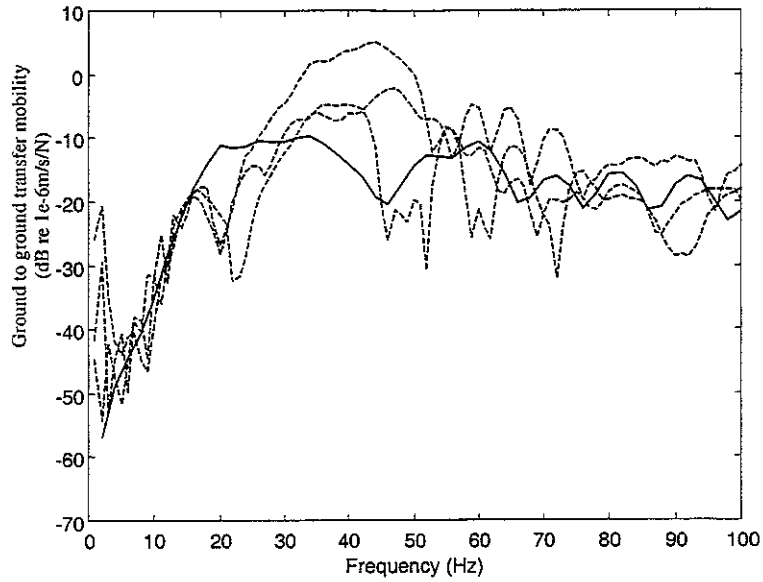

Figure 35. Transfer mobility of the ground surface (vertical component) at 10 m from the loading point on the ground surface. ——, predicted; – – –, measured.

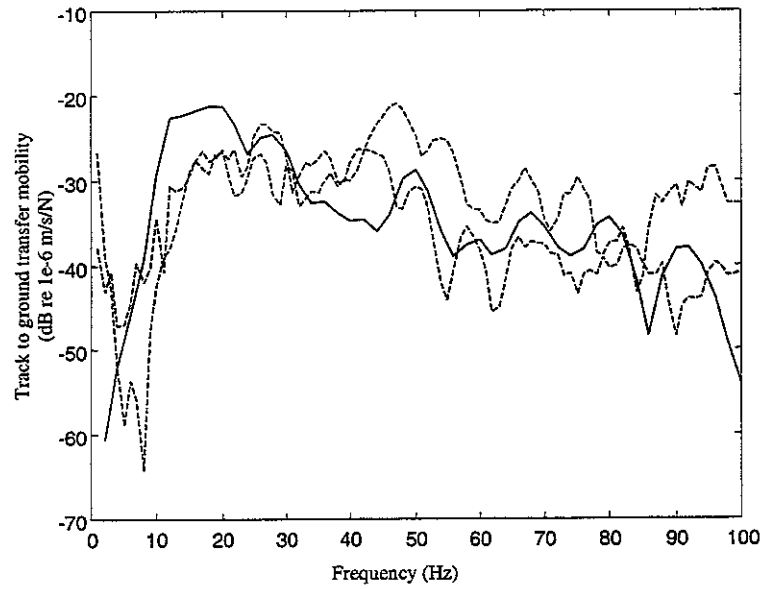

Figure 36. Transfer mobility from track to ground surface (vertical component) at 10 m from the near rail. ——, predicted; – – –, measured.

Figure 37 shows the predicted vertical velocity levels at a distance of 10 m from the track for different embankment Young's moduli and different track/ground contact widths. Also shown in bold lines are the maximum and minimum levels derived from measurements of vibration from HAA wagons reported in reference [10]. Since the ground is relatively soft, modification of the track parameters has a great effect on the

response levels for frequencies higher than 10 Hz. The predicted level due to the quasi-static loads is lower than 40 dB and therefore is not shown in this figure.

The comparison of measured and predicted spectra at this site are good, especially noting the scale on the velocity axis of figure 37 compared to that of earlier figures. The calculated spectra generally lie within the range of measurement for the frequencies 4 Hz one-third octave band and above. The range of the measured data may be due in part to differences in out-of-roundness of the wheels. No account of this has been taken into the prediction.

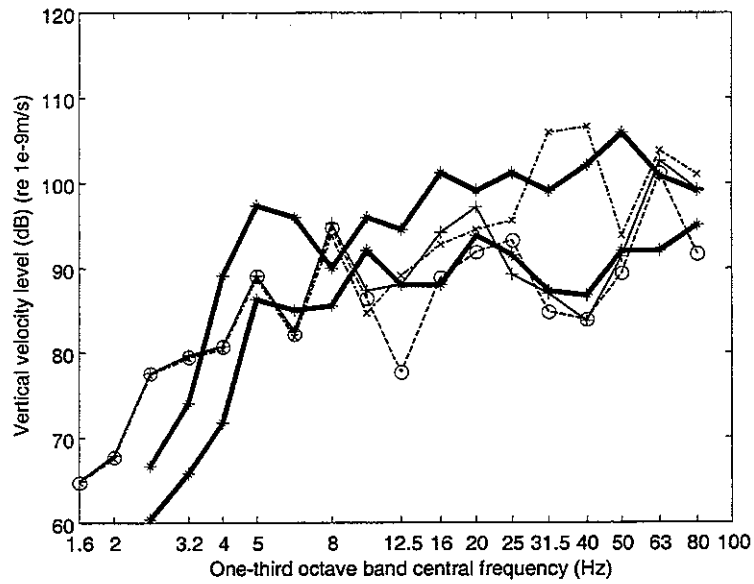

Figure 37. Vertical velocity levels at 10 m from the track at site Burton Joyce when five HAA wagons run at 14 m/s. +: the Young's modulus of the embankment is 1.5×10^7 N/m^2 and the track/ground contact width is 4 m; o: the Young's modulus of the embankment is 1.5×10^7 N/m^2 and the track/ground contact width is 5 m; ×: the Young's modulus of the embankment is 3.0×10^7 N/m^2 and the track/ground contact width is 4 m; *: maximum and minimum measured levels.

6. CONCLUSIONS

The prediction of the quasi-statically and dynamically induced vibration components has been carried out for three sites. The dynamically induced vibration prediction requires the knowledge of the vehicle dynamics and measurements of the vertical profile of the track. Site-specific data for the latter was only available to the authors for the third site. For the first two sites typical data has been used.

In the case of the first site, Ledsgård, the ground is not only unusually soft, but also unusual in that the second layer is softer than the surface layer. The measured displacement at the track has been shown to be close to that predicted for the quasi-static axle loads of the train both in the case of the train speed below, and above, the speed of the wave in the ground/embankment (figures 10 and 11). For the lower train speed (70 km/h), the dynamically induced vibration dominates the spectrum of vibration on the ground surface away from the track (figures 21 and 22). However, when the train speed exceeds the speed of the ground wave, a high level of vibration is observed in which the quasi-statically induced vibration dominates. At 7.5 metres from the track, this vibration is approximately 25 dB higher than the vibration observed for the lower speed. Vibration that is observed at long distances from the track has strongest components in the frequency range from about 3 to 8 Hz (e.g. figure 19). This is due to a combination of the facts (1) that at 200 km/h (55.6 m/s) the axle-loads excite the first mode of propagation at these frequencies (figure 4) and (2) that the mode shape of the first propagating wave changes considerably with frequency. Close to 3 Hz it has its maximum at the ground surface but at frequencies significantly below and above this, the displacement is strongest at the second layer interface below the surface (figures 6 to 9). The predicted level of the dynamically induced vibration appears to be too low. However, this prediction is based on vertical profile data taken from good track that may not be appropriate for a track that has been subjected to high dynamic displacements.

The second site, Via Tedalda, comprises a relatively stiff soil and therefore is very different from Ledsgård. As a consequence, the measured levels of vibration are much lower. The model predicts the rise in the measured vibration level that occurs in the frequency range from about 8 to 16 Hz (figures 27 and 28). This is due to the cut-on of the propagating mode of vibration at 12 Hz (figure 26). Although the train is capable of high speed, the measurements at this site are for a train speed that is lower than the first mode of propagation in the ground. For the measurement distances at 13 and 26 m from

the track, the observed vibration is demonstrated to be due to the dynamic generation mechanism. An over prediction of the dynamically induced vibration occurs near to the cut-on frequency of vibration in the layer. This is due to the fact that the ground is modelled as a distinct layer with a change of stiffness at exactly 10 m depth. The stiffness of the embankment is not known. Results show that the predicted levels are sensitive to this parameter for the frequency range in which propagation takes place in the upper layer (and the track). Notwithstanding the uncertainty in the embankment stiffness and the vertical track profile data that has been used, the model predicts the vibration level well for most of the frequency range except for 2.5 Hz to 5 Hz (figures 27 and 28). No satisfactory explanation for the under-prediction in this range has been found.

At the first two sites, measurements were made for high-speed passenger rolling stock. Measurements for two-axle freight wagons were made at the third site, Burton Joyce. Here there are fairly soft soil conditions with the speed of the first propagating wave in the ground tending towards 77 m/s at high frequency (i.e. the 'Rayleigh' wave speed). As well as the specifically measured vertical profile of the track, measured data consisting of transfer mobility measurements for the ground only, and from the track to the ground, are available. These have been used to validate the ground model and track/ground model at intermediate stages before the comparison of measurements of train-induced ground vibration (figures 35 and 36). Additionally, at this site, some indication of the range of measurement levels for different trains is available. This variation, in itself, suggests that a much closer correspondence with predictions than has been obtained from the model, would not be significant. In the present analysis no variation between trains has been included since wheel irregularity data (and other variation, e.g. loading, vehicle condition) has not been available. With some uncertainty in the parameters for the embankment and the effective width that should be used for the contact of the track structure with the ground, the levels predicted are close to, or within, the band of levels of train measurements (figure 37). The predicted level due to the quasi-static loads is much lower than this band. Thus in the vibration observed at this site, the dynamic component of vibration is, once more, the dominant one.

The comparisons of measured and predicted vibration at the first site show that the model may be used to study the effects of high-speed trains running on very soft soils. The comparison at the second site extends the validation to a relatively stiff soil site and, despite the discrepancy at the low end of the frequency range of interest, shows that

the model predicts vibration levels relatively well. Uncertainties in the stiffness of the embankment lead to uncertainty in the prediction for frequencies above the cut-on of vibration in the soil layer that are of the same order of magnitude as the differences between the prediction and measurement. The third site extends the validation to freight rolling stock and confirms the role of uncertainties in the parameters. Apart from the case of the X2000 train travelling near to the speed of wave propagation in the ground, the results presented here show that the dynamic mechanism of vibration generation is the most important. For the X2000 train at 200 km/h at Ledsgård, the excitation of a propagating wave by the quasi-static axle loads is confirmed.

7. ACKNOWLEDGEMENTS

The authors are grateful to A. Smekal and Dr M. Li of the Swedish National Rail Administration (BANVERKET), Dr C. G. Lai (Studio Geotecnico Italiano S.r.l., Milano, Italy) and J. Block (AEA Technology, UK) and to their organisations for their provision of parameters and measured data.

REFERENCES

[1] Seminar on High Speed Lines on Soft Ground, Dynamic Soil-Track Interaction and Groundborn Vibration, 16-17 March 2000, Gothenburg, Sweden.

[2] N. Chouw and G. Schmid 2000. Proceedings of The International Workshop Wave 2000, 13-15 December 2000, Bochum, Germany.

[3] V. V. Krylov 1994 *Applied Acoustics* **42**, 199-213. Calculation of low frequency vibrations from railway trains.

[4] M. Petyt, C.J.C. Jones 1999 *Structural Dynamics-EURODYN'99*, 79-87. Modelling of ground-borne vibration from railway.

[5] H. Grundmann, M. Lieb and E. Trommer 1999 *Archive of Applied Mechanics* **69**(1), 55-67. The response of a layered half-space to traffic loads moving along its surface.

[6] X. Sheng, C. J. C. Jones and M. Petyt 1999 *Journal of Sound and Vibration* **228**(1), 129-156. Ground vibration generated by a load moving along a railway track.

[7] C. G. Lai, A. Callerio, E. Faccioli and A. Martino 2000 *Proceedings of the International Workshop Wave 2000*, 99-110. Mathematical modelling of railway-induced ground vibrations.

[8] Banverket report 1998 High-Speed Line on Soft Ground (in Swedish).

[9] C. J. C. Jones, X. Sheng and D. J. Thompson 2000 *Proceedings of the International Workshop Wave 2000*, 83-98. Ground vibration from dynamic and quasi-static loads moving along a railway track on a layered ground.

[10] C. J. C. Jones and J. R. Block 1996 *Journal of Sound and Vibration* **193** (1), 205-213. Prediction of ground vibration from freight trains.